Journal of
Mechanical
Science and
Technology

Journal of Mechanical Science and Technology 21 (2007) 1100~1111

On The Dependence of Spray Momentum Flux in Spray Penetration: Momentum Flux Packets Penetration Model

R. Payri*, S. Ruiz, F. J. Salvador, J. Gimeno

CMT-Motores Térmicos, Universidad Politécnica de Valencia Camino de Vera s/n, E-46022 Spain

(Manuscript Received July 14, 2006; Revised March 29, 2007; Accepted March 29, 2007)

Abstract

Momentum flux is a very important parameter for predicting the mixing potential of injection processes. Important factors such as spray penetration, spray cone angle, and air entrainment depend largely on spray momentum. In this article, a model is obtained which is able to predict the spray tip penetration using as an input the spray momentum flux signal. The model is based on the division of the momentum flux signal into momentum packets (fuel parcels) sequentially injected, and the tracking of them along the spray. These packets follow a theoretical equation which relates the penetration with the ambient density, momentum, spray cone angle and time. In order to validate the method, measures of momentum flux (impingement force) and macroscopic spray visualization in high density conditions have been performed on several mono-orifice nozzles. High agreement has been obtained between spray penetration prediction from momentum flux measurements and real spray penetration from macroscopic visualization.

Keywords: Spray; Penetration; Momentum flux; Model; Fuel parcel

1. Introduction

The objective of the fuel injection process in diesel engines is the preparation of the fuel-air mixture in order to achieve an efficient combustion process with low pollutants formation. This process is strongly influenced by the spray behavior which depends mainly on the spray momentum (Payri et al., 2005a). The spray momentum gives information about the mass flow rate and the flow exit velocity simultaneously, thus controlling the mixture of the fuel and the air together with the ambient density (Payri et al., 2005a; Desantes et al., 2006; Desantes et al., 2007). In recent years the trend in diesel engine design has been an increase in the ambient density (higher boost pressure) and of the spray momentum (higher injection pressure and the use of convergent nozzles).

In this paper a new algorithm based on the use of the experimental measurement of spray momentum in order to predict the transient behavior of the spray penetration is presented. The main contribution of this model, and what makes it different from previous empirical or semi-empirical equations in the literature (Dent, 1971; Koo, 1996; Naber and Siebers, 1996; Wakuri et al., 1960; Payri et al., 2005b; Yeom, 2003) is that it takes into account non-stationary conditions due to the dynamic behavior of the injector, specially at the beginning of the injection process (during needle lift), or possible injection pressure fluctuations.

In order to validate the model a wide experimental program is presented; three axi-symetrical convergent nozzles, three injection pressures and two discharge pressure (discharge densities) have been tested.

The paper is structured in six main sections. First the experimental setup and the test matrix are presented. The second and third section describe the spray momentum and the macroscopic spray visualization techniques and the results obtained with

*Corresponding author. Tel.: +34 96 387 9658, Fax.: +34 96 387 7659
E-mail address: rpayri@mot.upv.es

those capabilities. In the fourth section the penetration model is presented, which is validated in section five. In the last section, a study of the influence of momentum flux signal shape on the spray tip penetration is performed.

2. Experimental set-up

The injection system used was a conventional Common Rail Fuel Injection system (Flaig et al., 1999) which allows fuel injection under high (up to 180 MPa) and relatively constant pressure.

To perform this investigation three different mono-orifice sac nozzles have been used. In order to obtain the internal geometrical characteristics of the nozzles, a special methodology described in Macián et al.(2003) was used. This methodology is based on the use of a special type of silicone to obtain the internal moulds of the nozzle. Once the moulds have been obtained, pictures of them are taken with a microscope. This experimental tool is useful for the study of diesel nozzles, because it enables researchers to establish relationships between internal geometry, flow characteristics and spray behavior. The k-factor is an indicator of the nozzle conicity, and it is defined as:

$$k - factor = \frac{D_i - D_o}{10} \quad (1)$$

The diameters and the k-factor of the investigated nozzles obtained following the silicone methodology are shown in Table 1. As can be seen from the table, all nozzles are convergent, with high k-factors.

2.1 Spray momentum test rig

With this experimental equipment it is possible to determine the impingement force of a spray on a surface. This force is equivalent to the spray momentum flux. Figure 1 shows a sketch of the momentum test rig. Sprays are injected into a chamber that can be pressurized with nitrogen up to 8 MPa in order to simulate pressure discharge conditions that are representative of real pressure conditions inside the engine combustion chamber during the injection process.

Table 1. List of nozzle characteristics.

Name	D_{out} (μm)	k-factor
A	112	2.1
B	137	2
C	156	1.8

2.2 Macroscopic spray visualization: Nitrogen test rig.

For the macroscopic spray characterization, an injection test rig is used that reproduces both the high gas density and pressure encountered in a diesel engine combustion chamber. The test rig is pressurized with nitrogen and it basically consists of a constant volume vessel with optical access for visualization purpose. The design is modular, and ancillaries can be added depending on the required experiment. The rig is designed for a maximum gas pressure of 6 MPa.

It is necessary to circulate the nitrogen through the rig because otherwise the injected diesel would obscure the windows and severely degrade the quality of the images. Furthermore, it is important to keep rig pressure (Pb) and nitrogen temperature constant during each experiment. A sketch of the high pressure nitrogen test rig is shown in Fig. 2.

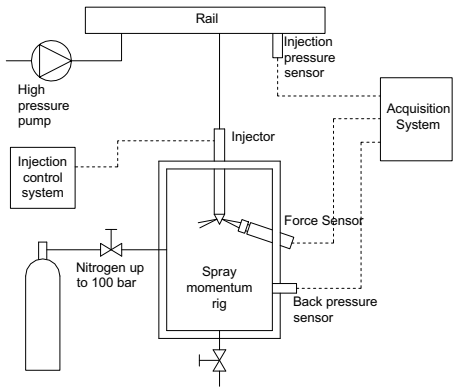

Fig. 1. Spray momentum test rig.

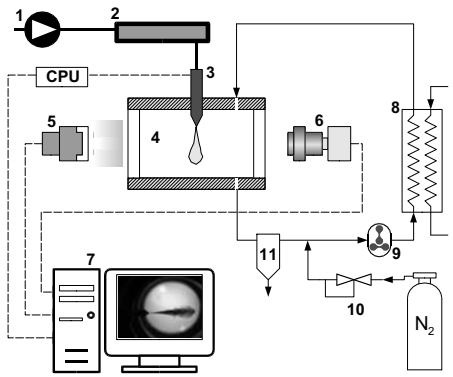

Fig. 2. Sketch of the nitrogen chamber configuration.

2.3 Image acquisition system and image processing software

The images are taken with a 12-bit color CCD camera with a spatial resolution of 1280 x 1024 pixels, and a minimum exposure time of 10 microseconds with a jitter of ± 5 microseconds. All the experimental equipment (camera-flash-injection) has been synchronized with an electronic system, by using the injector trigger signal as a reference signal to take the image sequences. In this study, spray visualization is carried out by using the back lighting technique (Pastor et al., 2001).

The injection is controlled with a modified ECU system that allows injection at a very low frequency (0.5 Hz). This low frequency is required for the nitrogen flow within the rig to be able to remove the fuel droplets from the previous injection and thus maintain good optical access to the spray.

The images were digitally processed using our own software. The segmentation algorithm used, based on the log-likelihood ratio test (LRT), has the advantage of using the three channels of RGB images for a proper determination of boundaries that are not well defined, as in the case of sprays. Details are available in Pastor et al.(2001).

2.4 Experimental conditions

Spray momentum flux measurements and macroscopic spray visualization have been performed at different experimental conditions, which are summarized in Table 2. Three different injection pressures (Pi) of 30, 80 and 130 MPa were tested. For each pressure and nozzle, two different values of back pressures (Pb) were used--2.5 MPa and 3.5 MPa--which considering the temperature inside the test rig constant and fixed at 25ºC, provides two different values of air density of 30 Kg/m^3 and 40 kg/m^3. In total, six different injection conditions per nozzle have been performed. An injection duration of 2 ms has been used in order to ensure a fully developed spray.

Table 2. Experimental conditions for the spray macroscopic characteristics and momentum flux measurements.

Nozzle	D_{out} (μm)	Pi [MPa]	Pb [MPa]	Density (kg/m^3)
A	112	30-80-130	2.5-3.5	30-40
B	137	30-80-130	2.5-3.5	30-40
C	156	30-80-130	2.5-3.5	30-40

3. Results

3.1 Momentum flux

The instantaneous momentum flux has been measured for the six tested points and the three nozzles. As an example, in Fig. 3 the instantaneous momentum flux from the three nozzles and for the injection pressures of 30 MPa and 80 MPa, and discharge pressure of 3.5 MPa is shown. Typical top hat profile can be observed during the time the needle is fully open. The small fluctuations at maximum needle lift are produced by pressure waves inside the injection line and the injector (Bermúdez et al., 2005; Kim and Lee, 2003). Furthermore, a dip can be seen in the momentum curves just after the beginning. It is produced mainly by the increase of effective injection pressure when the needle reaches its maximum position. This phenomenon typically appears in injection rate signals as well as spray momentum signals. As can be seen from the figures, the momentum flux increases when increasing either the diameter or the injection pressure (Payri et al., 2005a ; Payri et al., 2005b).

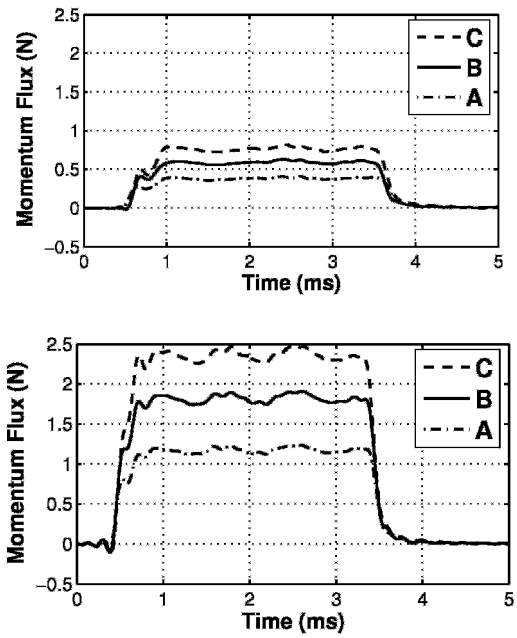

Fig. 3. Spray momentum flux for the three nozzles at Pi= 30MPa – Pb= 3.5MPa (upper part) and Pi= 80MPa – Pb=3.5MPa (lower part).

3.2 Spray visualization

The macroscopic parameters of the spray used for characterization are the tip penetration (S) and the spray cone angle (θ), represented in Fig. 4. The spray angle is considered as the cone angle which is formed by the spray considering 60 % of the penetration (Pastor et al., 2001). Five repetitions each 25 microseconds during an injection of 2 ms of duration were taken. The value used for the model is the mean value of these five repetitions in each time step. The standard deviation was small for the spray penetration and also for spray cone angle: for the penetration the maximum standard deviation was around 0.7 mm., and for the cone angle was 1º. Therefore, the error determining these macroscopic parameters was very small. In Fig. 5 some examples of spray pictures can be seen. From each picture, penetration and spray cone angle have been determined. In Fig. 6 results of these two variables are presented for Pi=30MPa and Pi=80MPa with Pb=3.5MPa in all cases.

As can be seen in the results, the higher the orifice diameter, the higher the penetration. The same conclusion is valid for the injection pressure: the

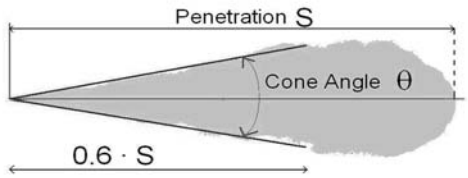

Fig. 4. Spray macroscopic characteristics.

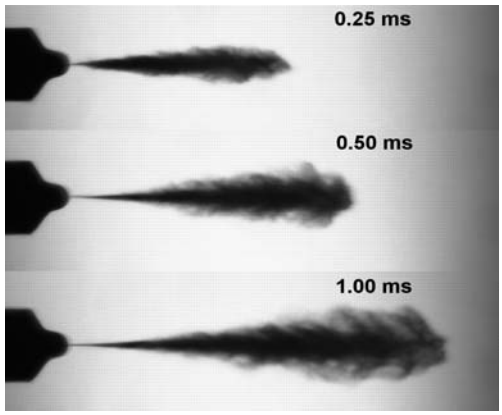

Fig. 5. Spray pictures. Nozzle B at point Pi=30 MPa – Pb=3.5 MPa (40 kg/m^3).

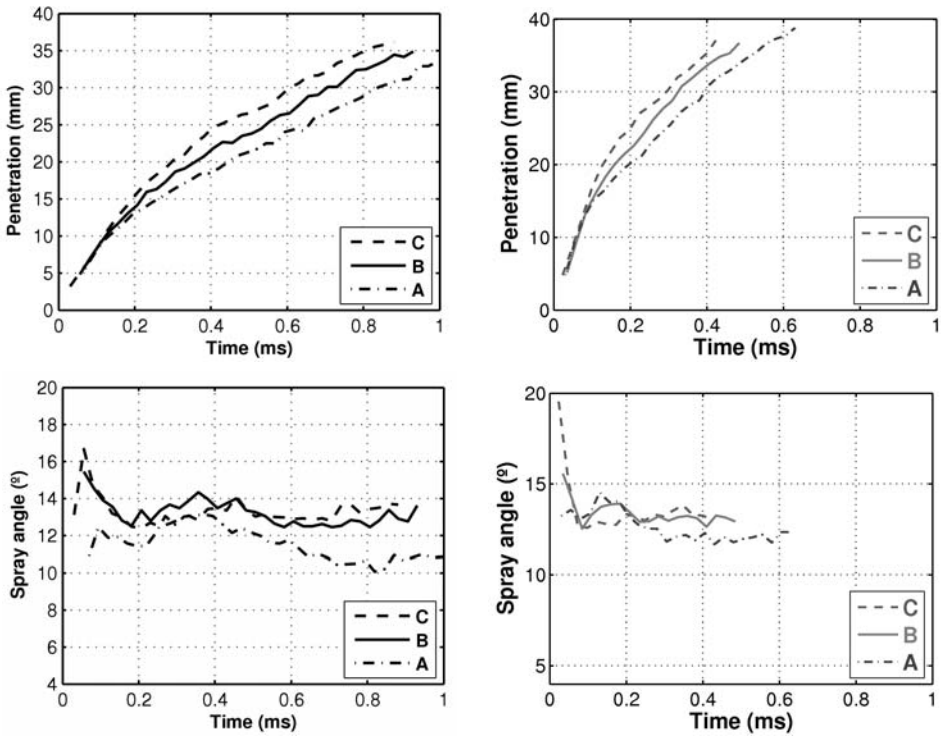

Fig. 6. Penetration and spray cone angle for the three nozzles at Pi=30MPa – Pb=3.5MPa (left) and and at Pi=80MPa – Pb=3.5MPa (right).

higher the injection pressure, the bigger the penetration.

The spray cone angle presents small variations during the injection, and for the three nozzles it is very similar. Since the model, which will be explained in the following section, needs as an input the spray cone angle, and considering its steady behavior, the mean value over the time will be considered.

4. Momentum packets penetration model

The model is based on a division of the momentum flux signal in momentum packets sequentially injected and the tracking of them from the time they are injected to the time they reach the tip of the spray. The division of the momentum flux signal can be seen in Fig. 7. These packets follow a theoretical equation which relates the penetration with the ambient density, momentum and time. The main point of the model is that the momentum flux that controls a given packet inside the spray is due to the addition of its momentum flux and the momentum flux of the previous packet. This packet moves forward inside the spray until it reaches the spray tip and it becomes the new leader packet. The packets which are leading the tip of the spray, and so, describing the penetration of the spray, penetrate against stagnant air only with its own momentum flux.

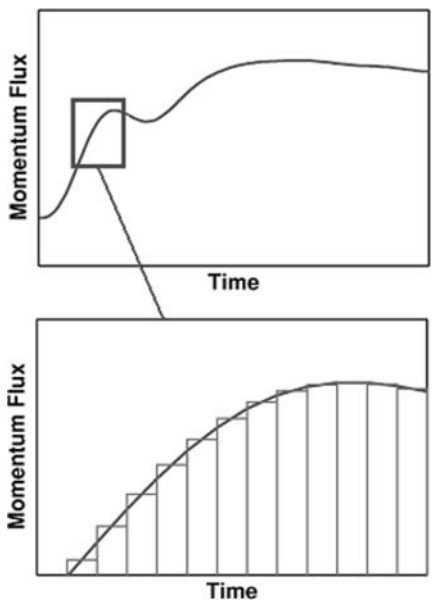

Fig. 7. Division in packets of the momentum flux signal.

Since the model is based on sequentially injected momentum packets (rectangular injections of constant momentum flux), it is necessary to determine an equation that relates the penetration and momentum at these conditions. Looking at the studies performed on this area (Wakuri et al., 1960; Dent, 1971; Naber and Siebers, 1996; Payri et al., 2005b), it is possible to find different semi-empirical models that relate penetration with parameters related to the injection system (injection pressure, diameter) and parameters related to the environment where the spray is injected (gas density). A theoretical expression can be obtained by performing a dimensional analysis with the following variables: ambient gas density, time from the start of injection and instantaneous momentum flux (Payri et al., 2005b). This dimensional analysis leads to an equation model, Eq. (2) that relates penetration with air density and spray momentum:

$$S(t) = cte \cdot \rho_a^{-1/4} \cdot \dot{M}_o^{1/4} \cdot t^{1/2} \tag{2}$$

where taking into account the spray cone angle, the *cte* can be expressed by:

$$cte = k_p \cdot \left(\tan\frac{\theta}{2} \right)^{-1/2} \tag{3}$$

Where ***kp*** can be considered a constant value independent of injection conditions or nozzle geometry. In a previous work a value for ***kp*** equal to 1.3 has been found for a quite large set of nozzle diameters and injection conditions (Desantes et al., 2006).

The momentum flux brings together the effective flux velocity at the orifice outlet, the fuel density and the effective diameter of the nozzles' orifices; and it can be expressed as (Payri et al., 2005a):

$$\begin{aligned} \dot{M}_o = \dot{m}_f \cdot U_0 &= C_a \cdot \frac{\pi \cdot \phi_o^2}{4} \cdot \rho_f \cdot U_o^2 \\ &= C_a \cdot \frac{\pi \cdot \phi_o^2}{4} \cdot \rho_f \cdot C_v^2 \cdot U_{th}^2 \end{aligned} \tag{4}$$

where $\dot{m}_f$ is the instantaneous mass flow rate, U_o is the effective outlet velocity, U_{th} is the Bernoulli theoretical velocity, and C_a and C_v are the contraction coefficient and velocity coefficient, respectively (Payri et al., 2005a).

Introducing Eq. (4) in Eq. (2) and applying the Bernoulli equation through the nozzle hole in order to obtain the velocity in terms of pressure drop, the spray tip penetration is given by:

$$S(t) \alpha \, \rho_a^{-1/4} \cdot \Delta P^{1/4} \cdot \phi_o^{1/2} \cdot t^{1/2} \tag{5}$$

Hence the dependencies found are those proposed by Hiroyasu (for a developed spray), Wakuri, and Dent (in this last case without the fuel evaporation term).

4.1 Spray axial momentum conservation

In order to understand how the model works it is necessary to take into account the fact that momentum is conservative in the axial direction. It means that the value of the axial momentum flux at the nozzle exit is the same as at any other cross-section of the spray axis. This fact is easily demonstrable in a stationary spray making few reasonable assumptions. In Fig. 8 a stationary spray is represented where a cylindrical control volume (CV) has been defined. One of the faces of the control volume contains the orifice outlet, and the other is located in any axial section of the spray. Two assumptions are made: first, pressure is uniform; second, air goes into the spray with a velocity component which is perpendicular to the axis of the spray. By applying the momentum conservation equation in these conditions, the axial momentum flux in any section along the spray is constant and equal to the momentum flux at the nozzle outlet. Obviously, the farther from the origin, the lower the axial velocity, but nevertheless, this velocity decrease is compensated for with a bigger spray cross-section and bigger total mass flow (fuel and air) due to air entrainment. Figure 9 (left) shows a sketch of the spray momentum measuring principle. The impact force is measured with a calibrated piezo-electric pressure sensor in order to measure force. The sensor frontal area and position are selected so that the spray impingement area is much smaller than that of the sensor. Under this assumption, and due to the conservation of momentum, the force measured by the sensor is the same as the momentum flux at the hole outlet or at any other axial location, since the pressure inside the chamber is constant and surrounds the entire spray, and deflected fuel flows perpendicular to the axis of the spray. The momentum conservation in the axial direction is experimentally confirmed in Fig. 9 (right) where the momentum flux signal (force) is shown for a given nozzle, and for an

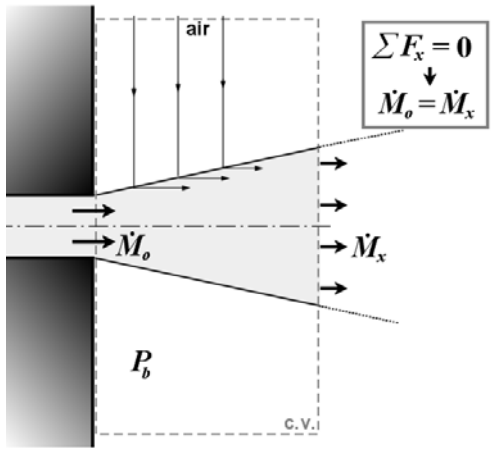

Fig. 8. Momentum conservation in a stationary spray.

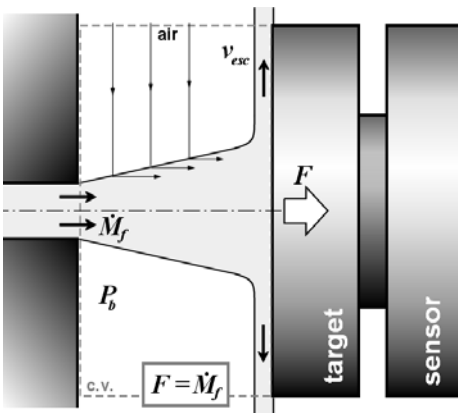

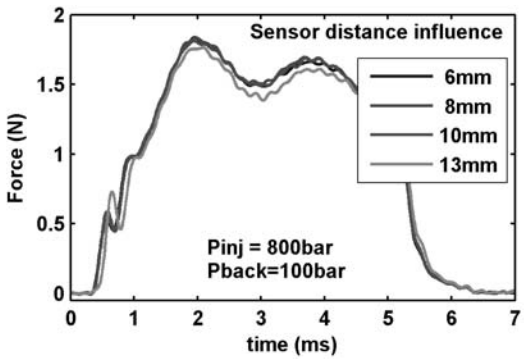

Fig. 9. Spray momentum measurement principle and momentum conservation.

injection pressure and back-pressure of 80 MPa and 10 MPa, respectively, and at different axial positions of the sensor (6, 8, 10, and 13 mm.). Figures show that the momentum at different positions is the same, except for x=13 mm. where the section of the spray due to air entrainment is higher than the frontal section of the sensor.

The results obtained for the stationary spray can be extrapolated to a transient spray whenever the two previous assumptions are fulfilled. These conditions are specially fulfilled in the main cone shaped part of the spray (stationary part), being not so true in the tip of the spray.

4.2 Model development

In order to explain how the model works a simple case will be analyzed. It consists of two consecutive rectangular injections which can be considered as two packets: packet 1 and packet 2 with momentum flux of $\dot{M}_1$ and $\dot{M}_2$, respectively. The following explanation is graphically described in Fig. 10.

At the beginning, packet 1 is injected and it penetrates against stagnant air with its momentum ($\dot{M}_1$).

Therefore, taking into account Eq. (2), the penetration of the packet 1 is given by Eq. (6) and, moreover it coincides with spray front penetration, since it is the first packet (leader packet).

$$S_1(t) = cte \cdot \rho_a^{-1/4} \cdot \dot{M}_1^{1/4} \cdot t^{1/2} \tag{6}$$

This situation (only first packet injected) is shown in Fig. 11, for an arbitrary time ***t=t_I*** in Figure 10.

In this figure the axial momentum flux at any axial position is represented. As can be seen, the momentum flux has been considered constant and equal to $\dot{M}_1$ inside the spray, since the spray momentum is conservative in the axial direction as stated in the previous section and taking into account two reasonable assumptions.

A time delay ***Δt*** after the first packet injection, packet 2 is injected. Nevertheless, the environment that it finds is very different than at the moment of the packet 1 injection. In fact, unlike packet 1, packet 2 finds air in movement due to the previous injection of packet 1, so packet 2 moves forward inside the spray faster than the previous packet. This new situation is depicted in Fig. 12 for a ***t=t_II*** in Fig. 10. In such a situation, packet 2 has a momentum flux, $\dot{M}_2$, but it moves forward inside the spray where the flow has a movement characterized by momentum $\dot{M}_1$ which has been transferred by packet 1. Thus, it can be assumed that packet 2 develops inside the spray as if it had a total momentum $\dot{M}_1 + \dot{M}_2$. Line 2' in Figure 10 represents this behavior which is governed by Eq. (7):

$$S_2'(t) = cte \cdot \rho_a^{-1/4} \cdot \left(\dot{M}_1 + \dot{M}_2\right)^{1/4} \cdot \left(t - \Delta t\right)^{1/2} \tag{7}$$

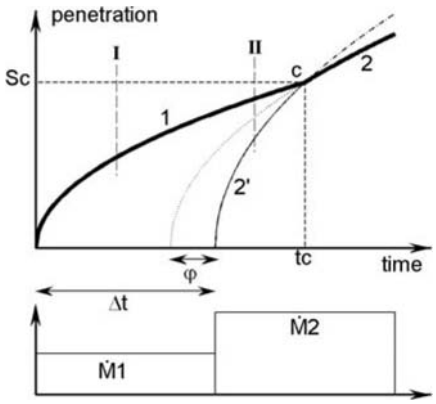

Fig. 10. Packet penetration model explanation.

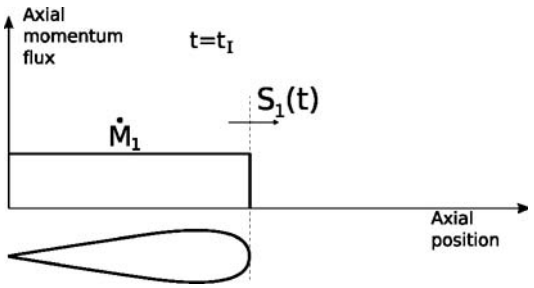

Fig. 11. Packet penetration model explanation. Development of packet 1 and axial momentum flux inside the spray.

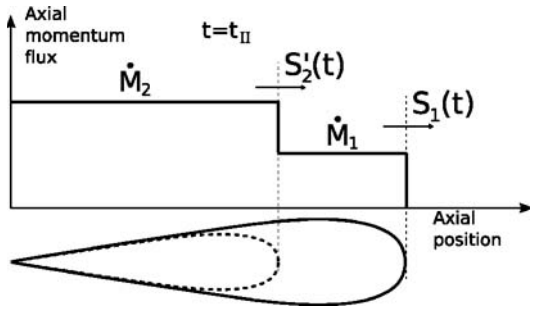

Fig. 12. Packet penetration model explanation. Development of packet 2 inside the spray and axial momentum flux.

With this situation, packet 2 reaches the front of the spray at point ***c*** (Fig. 10). The instant **tc** can be calculated by combining Eqs. (6) and (7). From this instant, packet 2 becomes the new leader packet and it develops against stagnant air, and so its penetration is governed by its own momentum flux $\dot{M}_2$. Taking this into account, from this point (***t>tc***) the development of the spray is controlled by Eq. (8). In order to ensure the continuity of the penetration at point ***c***, a phase lag, ***φ***, has to be considered in the equation. Physically it represents the difference in time as a result of the faster development inside the spray. This phase lag can be worked out making Eqs. (7) and (8) equal for t=***tc.***

$$S_2(t) = cte \cdot \rho_a^{-1/4} \cdot \dot{M}_2^{1/4} \cdot \left(t - \Delta t + \varphi\right)^{1/2} \quad (8)$$

This Eq. (8) is represented by line 2 in Fig. 10. The calculated spray tip penetration is represented by the widest line in Fig. 10.

This is a simple example of just two packets, but by proceeding in the same way and making use of a good signal discretization it is possible to calculate the spray penetration for real momentum flux measurements as shown in section five about model validation.

Full model formulation is included in the Appendix.

5. Model validation

In order to validate the model, the experimental penetration measurements have been compared with the model results. The model has been applied to each momentum flux signal and the mean value of the spray cone angle and a constant value for kp equal to 1.3 was used as additional experimental information, which is justified in Desantes et al.(2006).

Figure 13 shows a comparison between model and experimental penetration results for the three nozzles at Pi= 30MPa - Pb= 2.5 MPa and 3.5MPa (30 and 40 kg/m^3). The results at pressures of 80 MPa and 130 MPa are presented in Figs. 14 and 15 respectively. In these figures the experimental results are plotted with a cross line, and a discontinuous line is used for the model results.

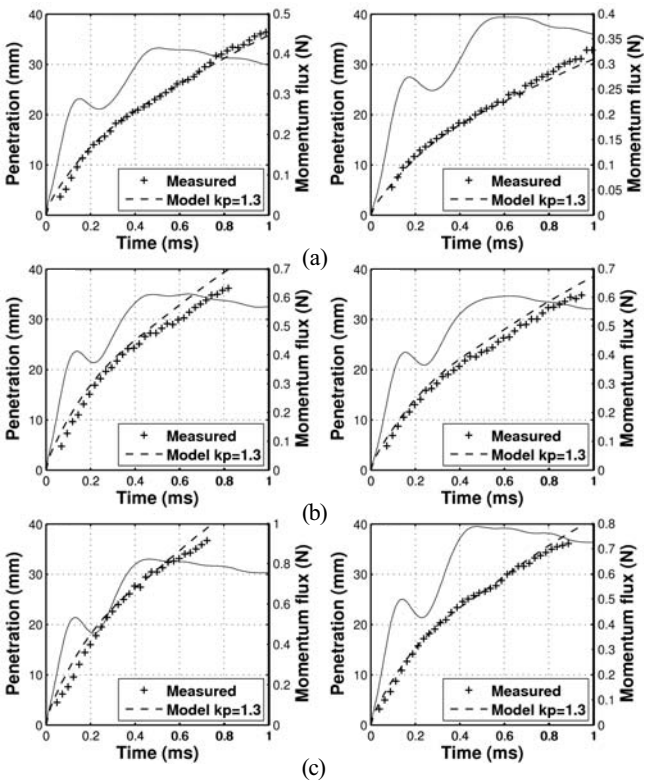

Fig. 13. Comparison between model and experimental penetration results for the three nozzles at Pi= 30 Mpa – Pb= 2.5 MPa and Pi= 30 Mpa – Pb= 3.5MPa (30 kg/m^3 and 40 kg/m^3).

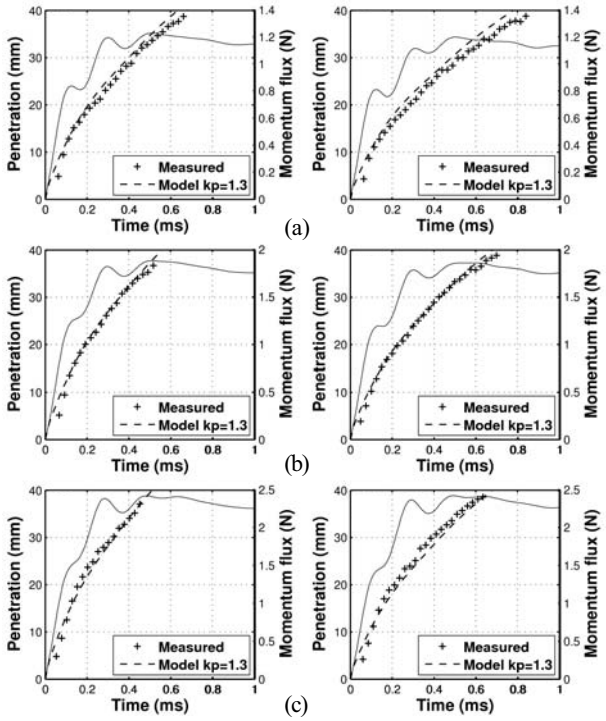

Fig. 14. Comparison between model and experimental penetration results for the three nozzles at Pi= 80 MPa – Pb= 2.5 MPa and Pi= 80 Mpa – Pb= 3.5 MPa (30 kg/m^3 and 40 kg/m^3).

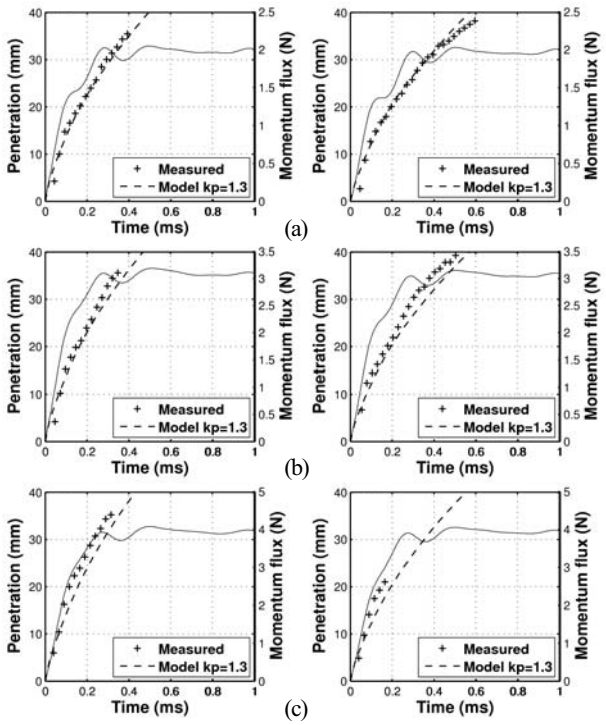

Fig. 15. Comparison between model and experimental penetration results for the three nozzles at Pi= 130 MPa – Pb= 2.5 MPa and Pi=130 MPa – Pb= 3.5 MPa (30 kg/m^3 and 40 kg/m^3).

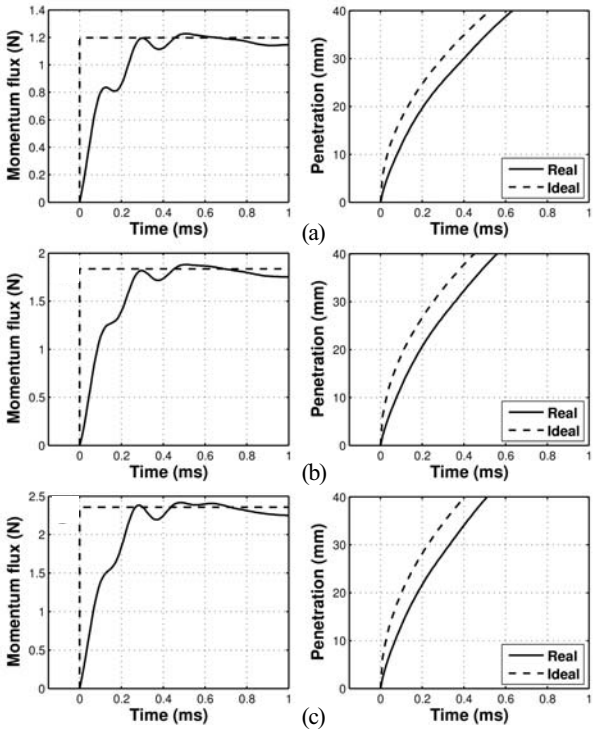

Fig. 16. Comparison between the penetration obtained from a real momentum flux signal and theoretical momentum signal. Results for the three nozzles at Pi= 80 MPa – Pb= 2.5 MPa.

The continuous line represents the spray momentum flux which is discretized in order to apply the model formulation. It is remarkable that the model takes into account the transient behavior of momentum: the momentum at the beginning of the injection is growing and there are also important fluctuations. In Figs. 13, 14 and 15, it can be observed how this momentum fluctuation is affecting the spray penetration behavior. Even in these circumstances the model is able to predict the dynamic behavior of the spray. In general, the agreement between model and experiments is very good except in some cases: under prediction for nozzles (b) and (c) at high injection pressures (130 MPa) and over prediction for nozzle (b) at low injection pressure (30 MPa).

6. Analysis of the influence of momentum signal characteristics on penetration behavior

Once the model is validated, in this section, the influence of the momentum signal characteristics on penetration is analyzed. As can be seen, from Fig. 3, experimental momentum signals differ from a theoretical momentum flux signal where momentum, and thus, injection velocity and mass flow rate are perfectly rectangular (constant) during the whole injection process. In real cases the needle lift is not instantaneous, and as a consequence, momentum is not rectangular and its shape changes for different injection conditions. This is due to the dynamic behavior of the injection system, which depends on the injection pressure. Also, a real momentum signal is affected by injection pressure oscillations due to pressure waves inside the injection line and the injector (Bermúdez et al., 2005).

In Fig. 16, the penetration obtained by applying the packets model to a real momentum signal is compared with the penetration obtained from the model when a theoretical rectangular momentum signal with the same maximum momentum flux value is considered. The curves represented belong to the point with 80 MPa of injection pressure and 2.5 MPa of backpressure. It is important to remark that in the theoretical case, the penetration obtained from the packets model is the same as the penetration obtained applying directly Eq. (3), which, as stated before, shows the same dependencies as other models considered in the literature Eq. (5). As can be seen

from the picture, the differences are important, and so the model presented can be used for predicting penetration taking into account real momentum signals.

7. Conclusions

■ The macroscopic spray characteristics and spray momentum flux from three different nozzles with different diameters have been evaluated in two different test rigs.

■ A theoretical model for the spray penetration in function of the time has been described.

■ The model is based on the division of the momentum flux signal in momentum packets sequentially injected and the tracking of them inside and at the tip of the spray.

■ These packets follow a theoretical equation which relates the penetration with the ambient density, momentum and time.

■ The main point of the model is that the momentum flux, which controls a given packet inside the spray, is due to the addition of its momentum flux and the momentum flux of the previous packet. This packet moves forward inside the spray until it reaches the spray tip and becomes the new leader packet. The packets which are leading the tip of the spray, and so, describing the penetration of the spray, penetrate against stagnant air only with its own momentum flux.

■ What makes this model different from previous empirical or semi-empirical equations in the literature (Dent, 1971; Koo, 1996; Naber and Siebers, 1996; Wakuri et al., 1960; Payri et al., 2005b; Yeom, 2003) is that it takes into account non-stationary conditions due to the dynamic behavior of the injector, especially at the beginning of the injection process, i.e., during needle lift.

■ The momentum flux measurements for different test points have been used as an input of the model in order to predict spray penetration. The spray tip penetration predicted by the model has been compared in all cases with the experimental penetration obtained from the injection test rig.

■ The comparison has shown the ability of the model to predict the penetration even for the first time intervals.

Acknowledgments

The authors would like to thank José Enrique del Rey * for his collaboration in the experimental measurements. This research has been funded in the frame of CAVISPRAY project; reference GV06/060 from Generalitat Valenciana.

(*) From CMT-Motores Térmicos. Universidad Politécnica de Valencia.

Nomenclature

D_{in}	: Inlet diameter of the nozzle's orifices.
D_{out}	: Outlet diameter of the nozzle's orifices.
$k\text{-}factor$	: Convergence or divergence factor.
$\dot{M}$	: Momentum flux.
Pb	: Backpressure.
Pi	: Injection Pressure.
S	: Spray tip penetration.
T	: Time.
k_p	: Penetration constant.
S_i	: Packet penetration at the front of the spray.
S_i'	: Packet penetration inside the spray.
to_i	: Packet origin time.
tc_i	: Packet front reaching time.
Sc_i	: Packet front reaching penetration.

Greek symbols

ρ_a	: Ambient density.
θ	: Spray cone angle.
φ_i	: Packet phase lag.

References

Bermúdez, V., Payri, R., Salvador, F. J. and Plazas, A. H., 2005, "Study of the Influence of Nozzle Seat Type on Injection Rate and Spray Behavior," *Proc. ImechE*, Vol. 219, part D: J. Automobile Engineering, pp. 677~689.

Dent, J. C., 1971, "A Basis for the Comparison of Various Experimental Methods for Studying Spray Penetration," *SAE Paper 710571*.

Desantes, J. M., Payri, R., Salvador, F. J. and Gil, A., 2006, "Development and Validation of a Theoretical Model for Diesel Spray penetration," *Fuel 85*, pp. 910~917.

Desantes, J. M., Payri, R., Garca, J. M. and Salvador, F. J., 2007, "A Contribution to the Understanding of Isothermal Diesel Spray Dynamics," *Fuel 86*, pp. 1093~1101.

Flaig, U., Polach, W. and Ziegler, G., 1999, "Common Rail System for Passenger car DI Diesel Engines," Experiences with Applications for Series Production Projects". SAE Paper 1999-01-0191.

Kim, C. H. and Lee, J. S., 2003, "An Analytical

Study on the Performance Analysis of a Unit-Injector System of a Diesel Engine," *KSME International Journal*, Vol. 17, No. 1, pp. 146~156.

Koo, J. Y., 2003, "The Effects of Injector Nozzle Geometry and Operating Pressure Conditions on the Transient fuel spray Behavior," *KSME International Journal*, Vol. 17, No. 3, pp. 617~625.

Macián, V., Bermúdez, V., Pyri, R. and Gimeno, J., 2003, "New Technique for the Determination of the Internal Geometry of Diesel Nozzles with the use of the Silicone Methodology," *Experimental Techniques*, Vol. 27, No. 2, pp. 39~43.

Naber, J. and Siebers, D. L., 1996, "Effects of Gas Density and Vaporisation on Penetration and Dispersion of Diesel Sprays," *SAE Paper 960034*.

Pastor, J.V., Arrègle, J., Palomares, A., 2001, "Diesel Spray Image Segmentation with a Likelihood Ratio Test," *Applied Optics*, Vol. 40, No. 17, pp. 2876~2885.

Payri, R., Molina, S., Salvador, F. J. and Gimeno, J., 2004, "A Study of the Relation Between Nozzle Geometry, Internal Flow and Sprays Characteristics in Diesel Fuel Injection Systems," *KSME International Journal*, Vol. 18, No. 7, pp. 1222~1235.

Payri, R., García, J. M., Salvador, F. J. and Gimeno J., 2005a, "Using Spray Momentum Flux Measurements to Understand the Influence of Diesel Nozzle Geometry on Spray Characteristics," *Fuel 2005*; 84: 551~561.

Payri, R., Salvador, F.J., Gimeno, J., Soare, V., 2005b, "Determination of Diesel Sprays Characteristics in Real Engine in-Cylinder Air Density and Pressure Conditions," *Journal of Mechanical Science and Technology*, Vol. 19, No. 11, pp. 2040~2052.

Yeom, J. K., "A Study on the Behavior Characteristics of Diesel Spray by using a High Pressure Injection System with Common Rail Apparatus," *KSME International Journal*, Vol. 17, No. 9, pp. 1371~1379.

Wakuri, Y., Fujii, M., Amitani, T. and Tsuneya, R., 1960, "Studies of the Penetration of a Fuel Spray in a Diesel Engine," *Bull. J.S.M.E. 3(9)*, pp. 123~130.

Appendix : Full model formulation

In this appendix is presented the full formulation of the model presented in this paper.

The penetration for the packet ***i*** when it is advancing inside the spray is shown in Eq. (1) where ***to*** is the injection beginning of the packet.

$$S_i' = cte \cdot \rho_a^{-1/4} \cdot \left(\dot{M}_{i-1} + \dot{M}_i\right)^{1/4} \cdot \left(t - to_i\right)^{1/2} \tag{1}$$

Once the packet reaches the spray front, its penetration formula will be:

$$S_i = cte \cdot \rho_a^{-1/4} \cdot \dot{M}_i^{1/4} \cdot \left(t - to_i + \varphi_i\right)^{1/2} \tag{2}$$

Operating with Eq. (1) applied to packet ***i*** and Eq. (2) applied to the packet (***i-1***), the point ***c*** (***tc*** and ***Sc***) where the packet i reaches the front can be calculated.

$$tc_i = \frac{\sqrt{\dot{M}_{i-1} + \dot{M}_i} \cdot to_i - \sqrt{\dot{M}_{i-1}} \cdot \left(to_{i-1} - \varphi_{i-1}\right)}{\sqrt{\dot{M}_{i-1} + \dot{M}_i} - \sqrt{\dot{M}_{i-1}}} \tag{3}$$

$$Sc_i = cte \cdot \rho_a^{-1/4} \cdot \left(\dot{M}_{i-1} + \dot{M}_i\right)^{1/4} \cdot \left(tc_i - to_i\right)^{1/2} \tag{4}$$

Finally, by operating Eqs. (4) and Eq. (2) considering ***t*** equal to ***tc*** is obtained the phase lag:

$$\varphi_i = \left[\sqrt{\frac{\dot{M}_{i-1} + \dot{M}_i}{\dot{M}_i}} - 1\right] \cdot \left(tc_i - to_i\right) \tag{5}$$

The model is getting data for previous packet so it is necessary to take into account that for the first packet ***to***, ***tc*** and $\boldsymbol{\varphi}$ are equal to zero.